Electrostatic Anchoring of Mn_4 Single-Molecule Magnets onto Chemically Modified Multiwalled Carbon Nanotubes

Concha Bosch-Navarro, Eugenio Coronado, Carlos Martí-Gastaldo,* Benito Rodríguez-González, and Luis M. Liz-Marzán*

Two different routes that enable the electrostatic grafting of cationic single-molecule magnets (SMMs) onto the surface of chemically modified anionic multi-walled carbon nanotubes (MWNTs) are described. The chemical nature and physical properties of the resulting hybrids are discussed on the basis of a complete battery of experimental techniques. The data show that the chemical nature of the SMM unit remains intact, while its magnetic response is significantly affected by the grafting process, which is likely due to surface effects.

1. Introduction

Single-molecule magnets (SMMs) constitute an active area of interest within the broader field of molecular magnetism.[1] These 0D systems are typically formed by magnetic clusters in which transition metal ions are connected through oxo ligands, and surrounded by capping organic ligands. More recently, analogous behavior has been observed in mononuclear complexes based on lanthanide ions.[2] Physical studies have demonstrated that these molecules behave like hard magnets at low temperature, and show interesting quantum phenomena. In view of these properties, SMMs are attractive candidates for molecular spintronics and quantum computing.[3] A key step towards implementing these systems in these exciting application areas is the deposition/grafting of SMMs onto suitable substrates, or their connection to electrodes. On the basis of their electronic properties, carbon nanotubes (CNTs) have been proposed as excellent substrates in this context,[4] because their electronic properties are highly sensitive to any change in their chemical environment, and because their extremely low spin–orbit and hyperfine couplings provide high-spin coherence lengths.[5]

A number of different routes have been exploited to drive the controlled organization of SMMs on CNTs. One of them exploits the robustness of the anionic polyoxometalate $[Fe_4(H_2O)_2(FeW_9O_{34})_2]^{6+}$ to mediate its assembly on purified single-walled nanotubes (SWNTs), producing a hybrid material that retains the magnetic bistability of the pristine SMM unit.[6] Other examples benefit from the chemical versatility of these unimolecular magnets, tailoring their organic shells and introducing functional groups that enable grafting on the sidewalls of the CNTs through strong supramolecular π–π interactions. For example, the assembly of a Fe(III) tetranuclear cluster $[Fe_4(L)_2(dpm)_6]$ (H_3L = 2-hydroxymethyl-2-(4-(pyren-1-yl)butoxy)methylpropane-1,3-diol; Hdpm = dipivaloylmethane) and a heteroleptic bis(phthalocyaninato) terbium(III) mononuclear complex incorporating a pyrene group in its periphery has been reported.[7] Nevertheless, before these systems can be successfully implemented into operational CNT-based nanoelectronic devices, several questions must be answered; namely, i) How does the grafting affect the magnetic properties of the SMMs, in terms of hybridization or environmental effects; ii) Which are the most suitable chemical interactions (i.e., covalent, supramolecular, electrostatic, etc) needed to drive the assembly of the molecular magnets without dramatically affecting the electrical conductivity of the CNTs.

In this work, we focus on two chemical routes enabling the electrostatic grafting of positively charged SMMs onto chemically functionalized anionic multiwalled nanotubes (MWNTs). As molecular nanomagnets we chose the cationic manganese(II, III) tetranuclear complex $[Mn_4(O_2CCH_3)_2(pdmH)_6]^{4+}$($Mn_4$) (pdmH = deprotonated pyridine-2,6-dimethanol)[8] because of its structural robustness and chemical versatility, which has been previously demonstrated through incorporation in several coordination frameworks whilst maintaining its intrinsic magnetic properties.[9] A full set of complementary techniques, including high-resolution electron microscopy (HRTEM), high-angle annular dark-field scanning transmission electron microscopy (HAADF-STEM), energy-dispersive X-ray spectroscopy (EDS), X-ray photoelectron spectroscopy (XPS) and conventional magnetometry, were used to demonstrate the success of the grafting process and to study the physical properties of the resulting hybrids.

2. Results and Discussion

2.1. Anchoring of the Mn_4 Molecules

To date, a number of different routes have been exploited to attach functional molecules onto carbon nanotubes. These

C. Bosch-Navarro, Prof. E. Coronado, Dr. C. Martí-Gastaldo[+]
Universidad de Valencia (ICMol)
Catedrático José Beltrán-2, 46980, Paterna, Spain
E-mail: eugenio.coronado@uv.es;
gastaldo@liverpool.ac.uk
Dr. B. Rodríguez-González, Prof. L. M. Liz-Marzán
Departamento de Química-Física
Universidade de Vigo
36310, Vigo, Spain
[+] Present address: Department of Chemistry, University of Liverpool, Crown Street, L697ZD, Liverpool, UK

DOI: 10.1002/adfm.201102227

have mainly focused on a) the formation of strong covalent bonds between prefunctionalized nanotubes and the molecular moiety of interest, b) the presence of weaker π–π supramolecular interactions between the aromatic sidewalls of the nanotubes and a predesigned molecule carrying a polyaromatic group, and c) electrostatic interactions between the nanotube and the molecular unit. Strategies (a) and (b) give rise to weakly coupled hybrids as they force the molecular cluster to reside far from the nanotubes, thus minimizing electronic interactions, while strategy (c) favors a more direct grafting of the molecular cluster onto the MWCNT, producing a stronger interaction. In this work we focus exclusively on this latter approach to attach the cationic Mn_4 cluster onto negatively charged MWNTs. As shown in **Scheme 1**, two different synthetic routes were followed in this context: 1) attachment through a two-step process, whereby the carboxylic groups are introduced to the outer walls of the MWNTs, and are subsequently deprotonated in basic medium, before being further linked in a second step to the cationic Mn_4 complex; and 2) direct attachment via a one-step process by combining the cationic complex with in situ generated anionic MWNTs.

The use of two different routes to accomplish a common goal stems from the different electronic effects that can be potentially introduced to the CNTs as a result of their functionalization. Note that the electrical conductivity of the resulting Mn_4-MWNTs hybrids is of utmost importance for the development of working CNT-based electronic devices. In this context, the first route will afford poorly conducting hybrids, as the carboxylic groups on the sidewalls of the CNTs are expected to behave as defects that disrupt the original sp^2 carbon electronic structure. On the contrary, the second approach should result in enhanced electrical conductivity of the hybrid relative to the pristine MWNT, as it involves n-type doping of the CNTs.

Route 1: Commercially available MWNTs were refluxed in a concentrated HNO_3 acid medium (further details can be found in the Experimental Section). According to previous works,[10] this process not only enables the introduction of carboxylic groups at the periphery of the nanotubes but also leads to removal of trace amounts of metal particles, which are commonly employed as catalysts in the production of CNTs, as well as amorphous carbonaceous forms present in the pristine material. In a first stage, the success of the functionalization was monitored through FTIR and thermogravimetric analysis (TGA). FTIR shows a broad band at 1115 cm^{-1} that corresponds to the C–O stretching mode (see Figure SI1 in the Supporting Information).[11] This band is merely residual in the pristine MWNTs, indicating the presence of more carboxylic groups in the post-functionalized material. Figure SI2 in the Supporting Information shows the thermal decomposition of these materials under ambient conditions. Whereas the pristine unmodified MWNTs

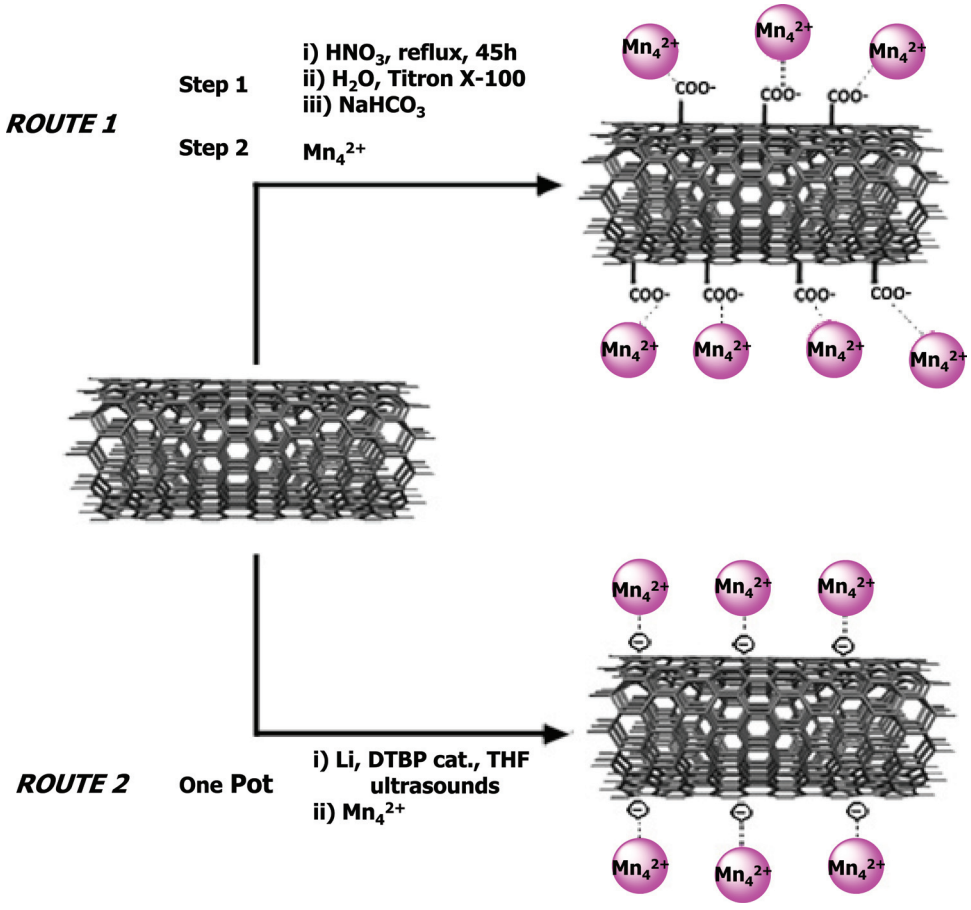

Scheme 1. Chemical routes used to electrostatically graft the positively charged SMM units onto chemically functionalized anionic MWNTs.

exhibit a single decomposition process around 550 °C that corresponds to the oxidation of carbon, the carboxylated material exhibits a more complex behavior, with two different mass-loss steps. The first, occurring between 300 and 400 °C and yielding a weight loss of 17%, can be associated to the coupled decomposition of the carboxylic groups connected on the CNTs and the Triton X100 surfactant molecules present in the medium. The presence of the surfactant was confirmed by atomic force microscopy (AFM) images, collected from casting a dispersion of the MWNT-COOHs onto a highly oriented pirolytic graphite (HOPG) surface (see Figure SI3 in the Supporting Information). This complex situation did not allow us to quantitatively estimate the percentage of carboxylic groups present in the sample; therefore we turned to indirect methods (vide infra). Upon heating, complete decomposition of the nanotubes was observed around 480 °C. This temperature is significantly lower than that recorded for the noncarboxylated material, as expected from the presence of a higher number of defects in the structure of the CNTs, which decrease their thermal stability.[12]

To determine the total percentage of acidic groups in the MWNT-COOHs, the nanotubes were back titrated (see Experimental Section). Assuming that all the acidic sites in our sample are carboxylic groups and that the sample is composed only of carbon atoms, this experiment yielded a percentage of 1.4%, which is in excellent agreement with other reported values.[13]

Finally, the deprotonated MWNT-COO^-s were suspended in acetonitrile, and the mixture was subjected to sequential ultrasonication cycles to achieve a homogeneous dispersion. Then, the Mn_4 clusters were added under continuous mechanical stirring. The presence of attractive Coulomb forces between the negatively charged walls of the MWNT-COO^- and the cationic $[Mn_4(OAc)_2(pdmH)_6]^{2+}$ units enables the grafting of the latter to produce the hybrid Mn_4-MWNT (**1**; Scheme 1). This grafting was preliminarily confirmed through TGA of **1**, which shows the formation of an oxide above 550 °C that represents approximately 50% of the sample weight, and was mainly composed of manganese, according to EDS analysis.

Route 2: Commercially available MWNTs were reduced by the addition of lithium, with DTBP (4,4′-di-tertbutyl-biphenyl) acting as a catalyst, to a suspension containing the nanotubes. This strategy permits the direct introduction of negative charges onto the sidewalls of the CNTs in a single step (further details can be found in the Experimental Section). The Mn_4 cluster was then carefully added to the mixture and anchored to the negatively charged MWNTs via attractive electrostatic interactions to produce the hybrid Mn_4-MWNT (**2**; Scheme 1).

The thermal decomposition of **2** under oxygen suggests the presence of several components in the sample. Mn_4 shows a complex thermogram with a number of decomposition steps. These steps can also be observed in the hybrid. The thermogram for **2** is even more complex, with the remaining mass being larger than that calculated by assuming a pure Mn_4-MWNT composition. This suggests the presence of DTBP, lithium, or intermediate species in the final hybrid, which is in agreement with the FTIR spectra (Figure SI1, Supporting Information). In light of this complex situation, the Mn_4 content in **2** cannot be directly determined from the TGA (Figure SI2, Supporting Information); its presence was again confirmed by EDS (vide supra).

2.2. Electron Microscopy and EDS Analysis

HRTEM images of the purified MWNTs and the Mn_4-MWNTs hybrids **1** and **2** were collected from specimens prepared by dropping freshly prepared dispersions in ethanol on carbon-coated copper grids.

Whilst the commercially supplied MWNTs are generally aggregated in weak-contrast bundles, accompanied by a significant number of dark spots associated with the remaining particles of the metal catalysts employed in their synthesis, the purified material exhibits a better dispersion of the nanotubes with a smaller number of interlocked junctions and no trace of high-contrast metal impurities (**Figure 1**).

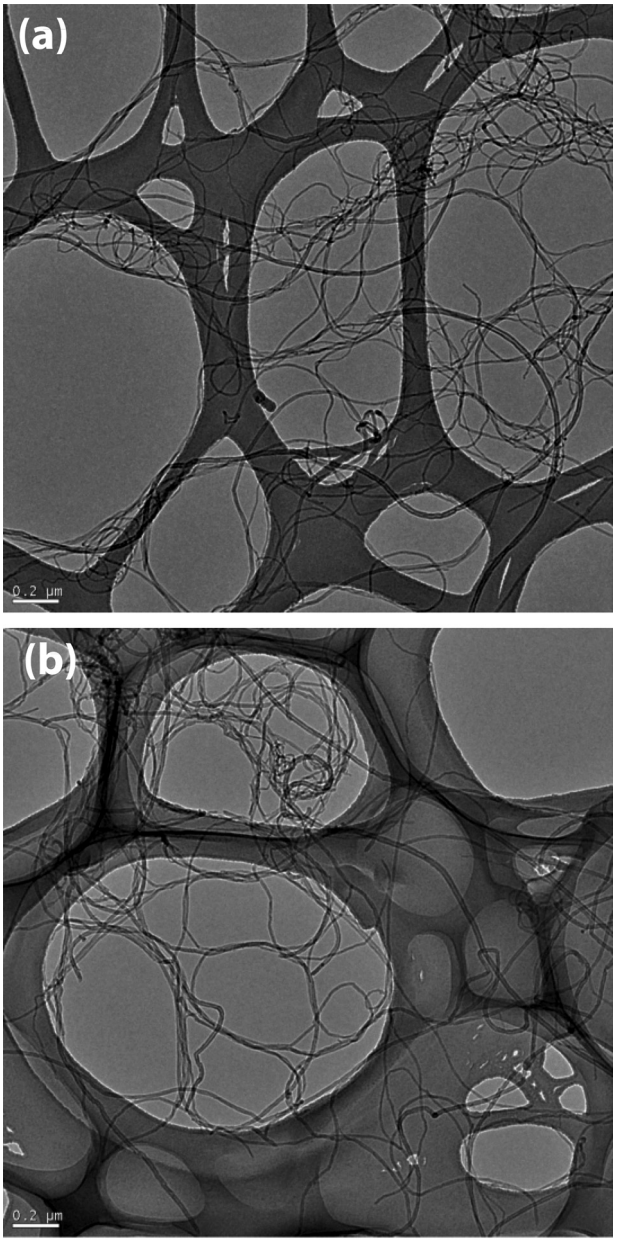

Figure 1. HRTEM images of the MWNTs as received from commercial suppliers (a) and after the acid treatment (b).

Route 1: A close look at the Mn_4-MWNT hybrid **1**, obtained from the addition of Mn_4 molecules to the prepurified carboxylate-containing nanotubes, reveals important differences with respect to the bare material (**Figure 2**a). At first glance, one can see some low-contrast material attached to the surface of the MWNTs, which is likely related to the grafting of the SMMs. Figure 2b displays a close up of one of these decorated MWNTs, which shows low-contrast objects attached to the surface of the nanotube of size ca. 1–2 nm, which is in excellent agreement with the dimensions of the molecular cluster. These objects are heterogeneously distributed along the nanotube's sidewall, with separations of 5–10 nm in some cases, while in others they tend to aggregate. Additional information regarding the chemical composition of the grafted objects was provided by EDS. Several spectra were collected from different areas across a single decorated MWNT, which confirmed that manganese was the only metal present and hence corresponds to the objects on the surface of the tube (Figure 2c; the copper signal observed can be attributed to the grid used to support the sample). Unfortunately, the manganese signal was too low to permit proper compositional mapping, which suggests that the grafting degree obtained by this procedure is poorer than that accomplished through route 2. This is in excellent agreement with the results obtained from XPS and the magnetic studies (vide infra), which also point toward a smaller amount of grafted material in **1**.

These high-resolution images also reveal the regular overlap of several planes (multiwall) along the nanotubes' sidewalls, confirming that their internal structure is maintained after functionalization and grafting of Mn_4 clusters (Figure 2a,b). This is of utmost importance, since the successful integration of such hybrids into CNT-based electronic devices is generally limited by the modification of the intrinsic transport properties of the nanotubes through the introduction of nonreversible structural damage.[14]

Route 2: Direct attachment of the Mn_4 clusters to the MWNTs, as reduced in situ, yields a homogeneous grafting of the molecular component. **Figure 3**a shows an almost regular distribution of grafted material on the nanotube's sidewall. This grafting behavior is likely induced by the presence of equally intense electrostatic repulsions between the positively charged clusters in the presence of a homogeneous distribution of negative charges along the nanotube wall. In this case the clusters exhibit the strongest contrast due to the greater thickness

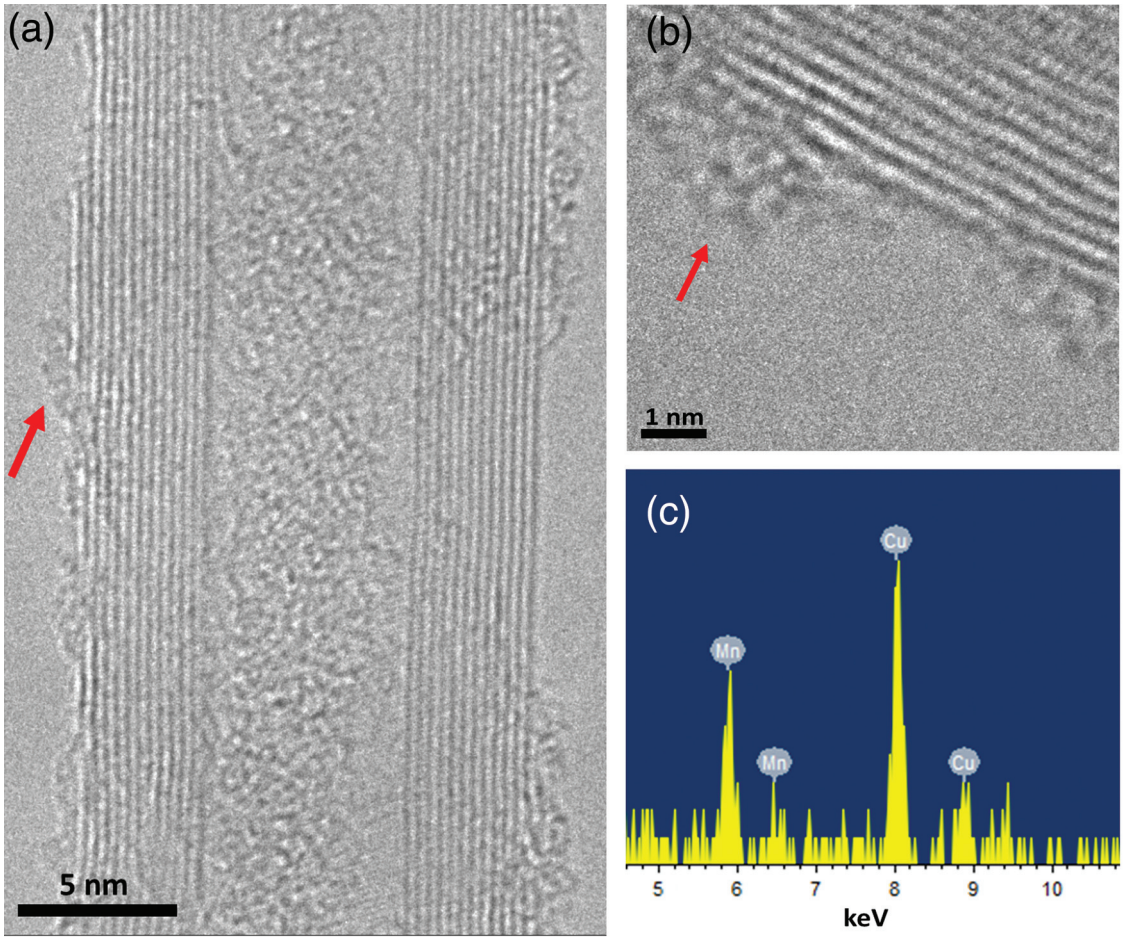

Figure 2. a,b) HRTEM images of 1 displaying the grafting of the Mn_4 complex (indicated by the arrows) on the surface of prefunctionalized MWNTs. The multiwalled structure of the CNTs can also be seen. c) EDS spectrum acquired from a single decorated MWNT like the one shown in (a), which confirms the presence of Mn. The Cu signal can be attributed to the TEM grid.

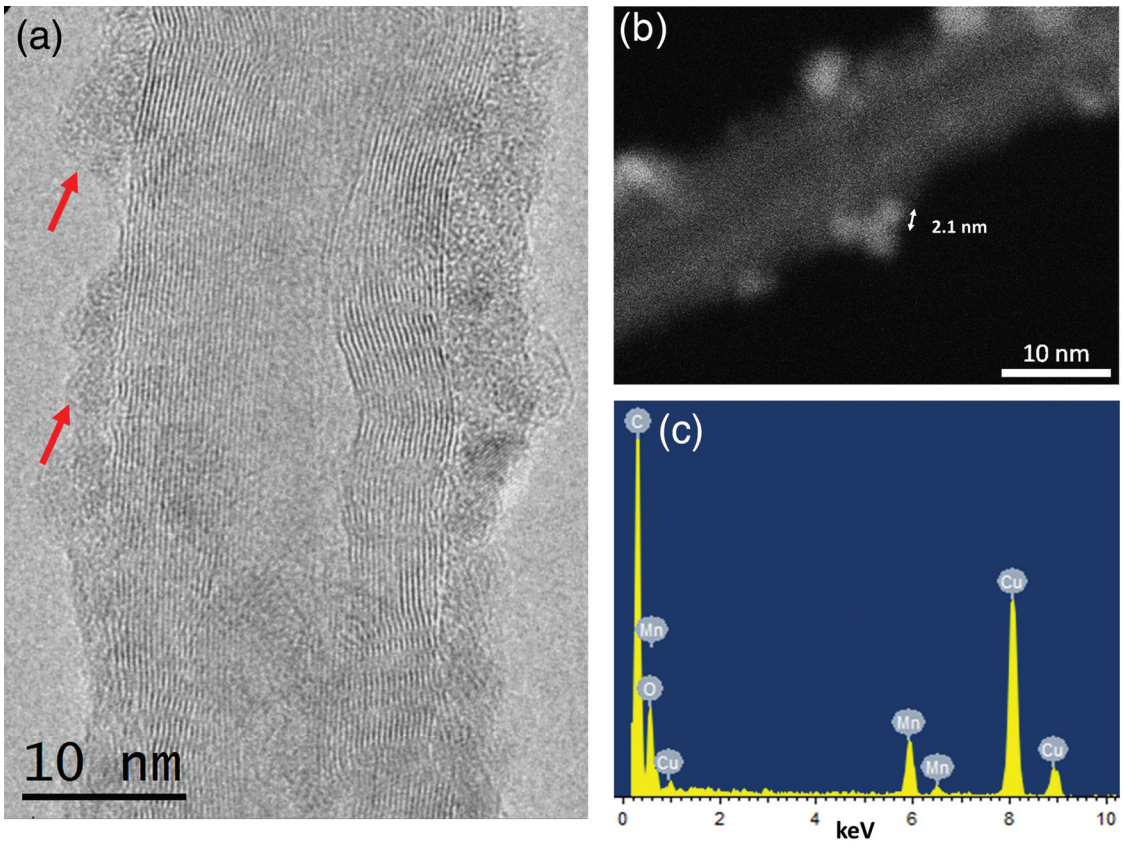

Figure 3. a) HRTEM images of **2** displaying the grafting of the Mn_4 complex (indicated by the arrows) on the negatively charged MWNTs. b) Z-contrast HAADF-STEM image showing the distribution of the clusters along the nanotubes (brighter spots) and their size (2.1 nm). c) Local area EDS spectrum confirming the presence of Mn on the MWNTs. Again, the Cu signal is attributed to the TEM grid.

of the attached material, which in some places almost forms a complete shell over the tube. The grafted material shows a globular arrangement with sizes ranging between 2 and 3 nm, which is again in good agreement with the size of the grafted molecular component. The Z contrast image confirms that these spheres are composed by high Z material (Figure 3b). The chemical nature of these moieties was corroborated by EDS analysis, which confirmed that (except for Cu arising from the supporting grid) Mn was the only metal present (Figure 3c). This point was further confirmed by STEM-EDS elemental mapping (**Figure 4**), which clearly shows the presence of units containing Mn surrounding the carbon nanotubes, in agreement with the bright spots identified in the Z-contrast HAADF-STEM image (Figure 3b).

2.2. XPS

XPS experiments provide evidence for all the elements expected to be present in the grafted MWNTs with binding energies in agreement with the expected bonding states. **Table 1** summarizes the bond energy (BE) values extracted from high-resolution spectra.

According to **Figure 5**, the Mn 2p (top) and Mn 3s (bottom) signals exhibited by the hybrids are in good agreement with the data collected from a crystalline sample of the Mn_4 complex, which is a strong indication of grafting success. In every case, the Mn 2p spectra (Figure 5, top) display two dominant peaks between 641 and 654 eV that can be assigned to the spin–orbit splitting into the $Mn(2p_{3/2})$ and $Mn(2p_{1/2})$ levels, with an energy splitting of ≈11.8 eV. Also, the $Mn(2p_{3/2})$ level is accompanied by a less intense satellite peak at higher binding energies (≈5 eV), in excellent agreement with that expected for the presence of Mn^{2+} ions.[15] This satellite contribution can be clearly observed for the Mn_4 blank and **2** whilst its presence is only marginal in **1**, which suggests a smaller number of grafted Mn_4 complexes in the latter. The Mn 3s region (Figure 5, bottom) displays an asymmetric doublet which can be ascribed to a multiplet splitting of ≈6 eV, in good agreement with the presence of Mn(II). Again, the Mn 3s spectrum of **1** exhibits a weaker and less defined signal than **2**, suggesting a minor degree of grafting. Additionally, the presence of Mn_4 in all the samples studied is confirmed by the nearly identical values of $\Delta E = [E(Mn_{2p1/2}) - E(Mn_{2p3/2})] = 11.72$ and 11.80 eV for pristine Mn_4 molecules and the hybrids **1** and **2**, respectively. ΔE values for other phases of manganese oxides such as MnO (5.5), Mn_2O_3 (10.5), Mn_3O_4 (11.3) or MnO_2 (11.9 eV) allows them to be ruled out.[16] Note that MnO_2 exhibits a ΔE value very close to that exhibited by the hybrids, but it can be excluded on the basis of the magnetic characterization (vide infra).

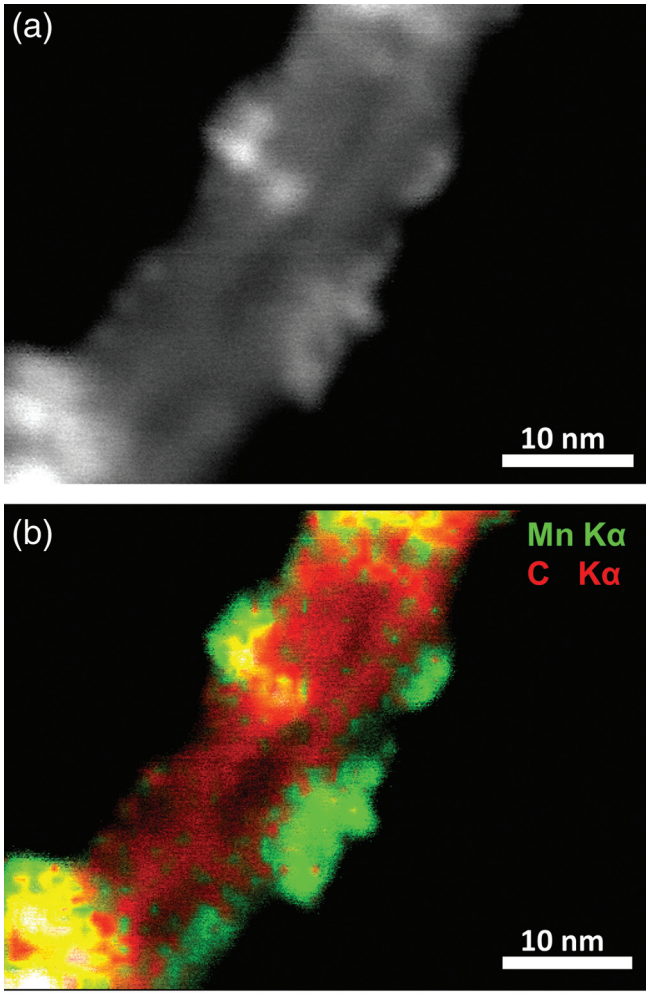

Figure 4. a) Z contrast HAADF-STEM image of Mn_4- MWNT hybrid 2. b) STEM-EDS elemental mapping performed over the area represented in (a) showing excellent agreement between the Mn distribution and the bright spots grafted to the nanotube.

Note that, except for Mn(II), which has the maximum number of unpaired d electrons, and accordingly exhibits the most intense satellite peaks, the identification of other oxidation states on the basis of XPS data has proven to be very difficult due to a slight influence of these Mn oxidation states on the BE shifts, and the broad nature of the collected peaks. Furthermore, the low concentration of the Mn_4 complex in the studied hybrids makes this task even more difficult due the poor signal/noise ratio.

2.3. Magnetic Measurements

Static magnetic properties of the purified MWNTs and the hybrids containing Mn_4 complexes were examined by studying the isothermal field dependence of their magnetization collected at 2 K (**Figure 6**). Bare purified nanotubes exhibit a ferromagnetic response, due to the presence of traces of metallic nanoparticles, reminiscent of the catalysts employed in their production. This behavior has been described previously, and reflects the difficulties inherent to the purification of carbon nanotubes.[17] The addition of Mn_4 complexes is clearly accompanied by an increase in the magnetic response of the hybrids with saturation values at 2.17 and 5.43 emu g^{-1} at 5 T, for **1** and **2**, respectively. The different responses exhibited by these two hybrids indicates that a greater degree of grafting is accomplished through the direct one-step metallization (route 2) in comparison with the two-step carboxylation/deprotonation process (route 1). This was anticipated on observation of the low-intensity Mn signals observed for **1** in the EDS and XPS experiments (vide supra). The less pronounced increase in magnetization of **1** and **2** at low fields with respect to the response exhibited by the bulk Mn_4 cluster seems to indicate that the polynuclear cluster might possess a different electronic structure when grafted to the nanotubes. In fact, previous reports have shown the direct relationship between the internal symmetry of the cluster (affected by the nature and number of solvate molecules accompanying the tetranuclear cluster) and its magnetic response.[8]

Alternating current (AC) dynamic magnetic measurements were carried out under an external applied field of 3.95 G (**Figure 7**). No out-of-phase signal was detected for **1** at the temperatures explored. This is attributed to the small number of Mn_4 molecules grafted through this route, which gives rise to a weak magnetic signal far below the sensitivity of conventional superconducting quantum interference device (SQUID) magnetometers. On the other hand, **2** exhibits an exponential increase in the in-phase signal (χ') which is accompanied by a positive response in the imaginary component below 5 K. Though the temperature limit does not permit observation of a maximum in the χ'' signal, the position of the susceptibility tails seems to be frequency dependent, as expected for a dynamic relaxation process. These features suggest the presence of a superparamagnetic state, which provides additional support for the presence of Mn_4 SMMs in the hybrid material. Still, clear differences between the hybrid **2** and the pristine Mn_4 are observed in the low T magnetic behavior. Hence, the blocking temperature for the latter appears at lower temperature, ca. 3.5 K, and exhibits a clearer dependence of the positions of the in-phase and out-of-phase peaks with respect to the frequency. Such a difference may be ascribed to small structural changes in the magnetic clusters when anchored to the MWNTs as result of distortion and loss of symmetry triggered by their contact with the carbon nanotubes. The presence of contaminant traces of manganese oxides that could be responsible for the magnetic response detected at low temperatures can be disregarded in

Table 1. Binding energies (BE) extracted from high resolution XPS spectra.

Sample	Mn 2p [eV][a]				Mn 3s [eV]		
	$Mn(2p_{3/2})$	$Mn(2p_{1/2})$	Δ_{BE}	$Mn(2p_{3/2})_{sat}$	Mn(3s)′	Mn(3s)″	Δ_{BE}
Mn_4	641.34	653.06	11.72	646.36	83.29	89.26	5.97
1	641.80	653.60	11.80	646.59	84.16	90.18	6.02
2	641.24	653.04	11.80	646.60	83.71	89.79	6.08

[a]Binding energy values referenced to $Si(2p_{3/2})$ (Si – Si) at 99.8 eV on an unsputtered surface.

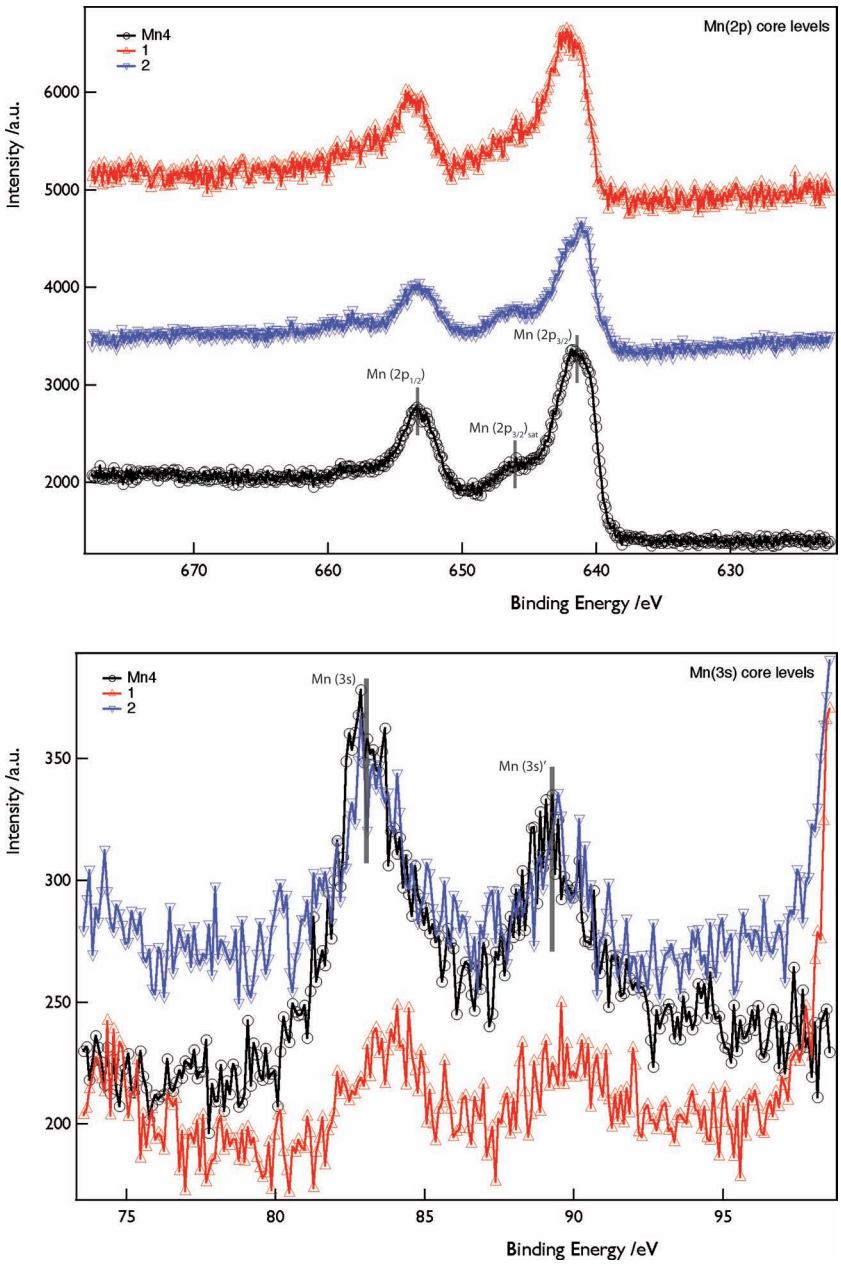

Figure 5. Core-level Mn 2p (top) and 3s (bottom) XPS spectra of the bulk Mn_4 complex (black circles) and the Mn_4-MWNTs hybrids (1: red triangles and 2: blue inverted triangles).

view of the data. In fact, Mn_3O_4 exhibits ferrimagnetic behavior below 43 K,[18] MnO behaves as an antiferromagnet with a Néel temperature of approximately 120 K,[19] while MnO_2 and Mn_2O_3 exhibit antiferromagnetic ordering below 84 and 90 K, respectively.[20]

3. Conclusion

A new method for the attachment of magnetic molecules (SMMs) to CNTs based on the electrostatic interactions is presented here. Our approach is in contrast with those reported so far, which have mainly focused on the chemical functionalization of the molecular component, while keeping the pristine CNTs intact. However, this strategy neglects the important effects that the chemical treatments used for the purification of the CNTs can have on their electronic properties. In fact, these treatments, which are crucial for the removal of the magnetic particles accompanying the carbonaceous material, generally lead to a residual functionalization of the CNTs and the introduction of scattering centers in their structure. On the other hand, these methods lead to hybrids in which the magnetic molecule is far away from the CNT. For this reason, we explored an alternative approach that relies on keeping the SMM unit intact and controlling the chemical functionalization of MWNTs (more robust than their single-walled counterparts) by introducing negative charges in their sidewalls through: 1) a two-step process, which includes the introduction of carboxylic groups and their subsequent deprotonation and 2) a one-step reduction of the CNT in the presence of a metal. Once negatively charged, the MWNTs can be readily grafted with the cationic SMMs through the presence of attractive Coulomb interactions in solution.

A first indication of the success of our method was provided by HRTEM and EDS, which show the attachment of manganese-containing molecular components whose size and composition are in good agreement with those expected for the Mn_4 clusters. Next, the chemical integrity of these nanometric objects after the grafting process was confirmed by XPS, which showed a good agreement between the spectra of the isolated hybrids and the response exhibited by the bulk Mn_4 complex. Finally, the magnetic response of the grafted molecules was studied with conventional magnetometry. From the saturation values of the isothermal field dependence of the magnetization we can conclude that route 2 produces a larger degree of grafting than 1. This is further confirmed by HRTEM images, EDS spectroscopy, and XPS experiments. In addition, the deviation of the M vs H curves and the dynamic AC susceptibility measurements with respect to behavior exhibited by the bulk Mn_4 cluster suggest that its magnetic response is significantly affected by the grafting process via surface effects.

Further work will involve an in-depth study of the electronic-transport properties of these hybrids, along with the use of single-walled carbon nanotubes. Additionally, we aim to introduce polyaromatic linkers into the organic shell of the Mn_4 cluster to enable its supramolecular grafting on CNTs, in agreement with commonly used methodology. The physical characterization of these complementary hybrids should

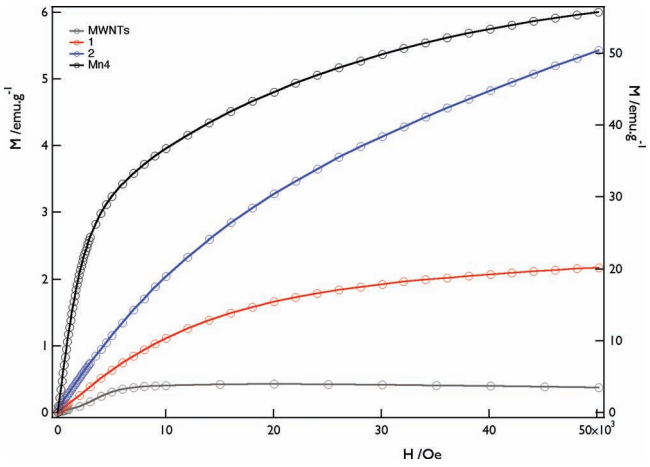

Figure 6. Isothermal field dependence of the magnetization of purified MWNTs (grey), Mn_4-MWNTs hybrids **1** (red) and **2** (blue), and nongrafted Mn_4 complex (black). Solid lines are a guide to the eye.

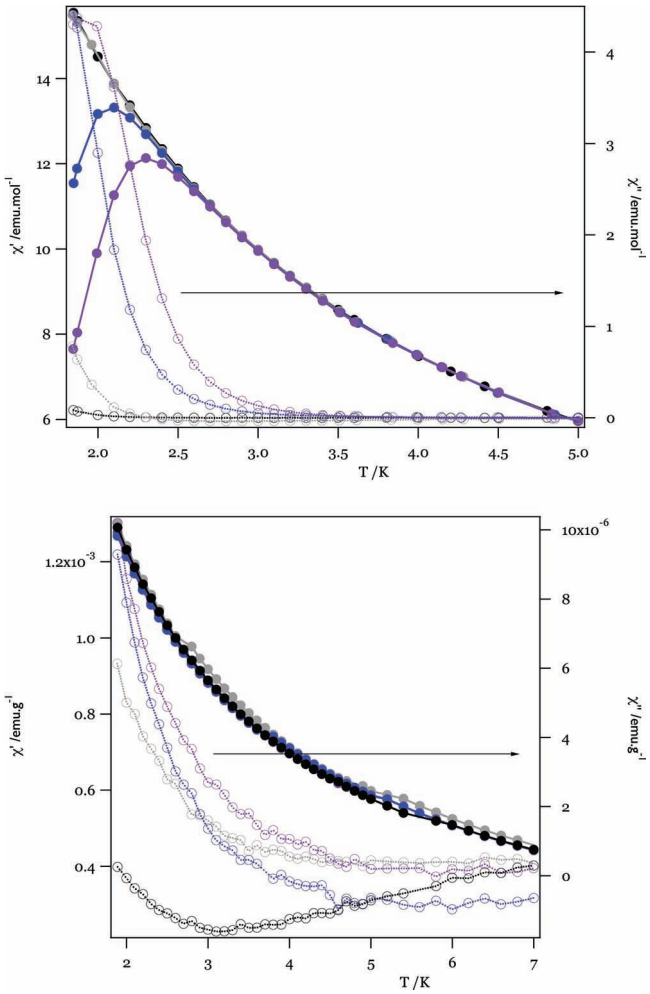

Figure 7. AC susceptibility of the hybrid **2** (top) and the pristine Mn_4 complex (bottom) collected in the 1 (black), 10 (grey), 110 (blue), and 333 Hz (purple) range. In-phase susceptibility and out-of-phase signals are represented by filled and empty symbols, respectively. Solid lines are a guide for the eye.

provide further insights into the environmental effects on the magnetic properties of this particular SMM when grafted onto nanotubes.

4. Experimental Section

General Synthetic Remarks: MWNTs were purchased from Thomas Swan & Co. (Elicarb MW-PR0940). Reactions requiring inert conditions were conducted under argon with oven-dried glassware (100 °C). Acetonitrile and tetrahydrofuran (THF) were dried over $CaCl_2$ and sodium, respectively; reagents were otherwise used as received. Samples were filtered by employing a vacuum filter funnel of pore size number 3, and either hydrophobic polytetrafluoroethylene (PTFE) membrane filters (0.45 µm pore size) or cellulose nitrate membrane filters (0.8 µm pore size). Ultrasound measurements were carried out with a Bransonic 5510E-MT operating at 135 W.

Synthesis of $[Mn_4(OAc)_2(pdmH)_6](ClO_4)_2$: The tetranuclear Mn cluster was synthesized according to the method previously described by Yoo et al.[8] with minor modifications. In a first step, $[Mn_3O(O_2CMe)_6(py)_3](ClO_4)$ (py = pyridine; C_5H_5N) was prepared as described elsewhere.[21] Next, this complex (1 g; 1.1 mmol) was dissolved in CH_2Cl_2 (75 mL) to afford a very dark brown solution. $PdmH_2$ (480 mg; 3.4 mmol) was then suspended in dichloromethane (75 mL) and gradually into the first solution. The slurry was mechanically stirred overnight at room temperature to allow complete precipitation of the cluster perchlorate salt. Finally, the insoluble fine brownish powder was separated from its deep-brown supernatant by filtering in vacuo and washing with dichloromethane until the filtrate was colorless. The solid was dried in vacuo overnight and recovered as an ochre powder. Anal. calc. (%) for $C_{46}H_{54}Cl_2Mn_4N_6O_{24}\cdot 2.5H_2O$ (M_W = 1365.6): N, 5.96; C 39.17; H, 4.22. Found (%): N, 5.80; C, 39.00; H, 3.97. FTIR (cm^{-1}): 3423.4 (m, br), 2913.1 (w), 2650.7 (w), 1604.5 (m, sh), 1578.3 (m, sh), 1462.4 (m, sh), 1445.8 (m, sh), 1387.0 (m, sh), 1330.6 (m, sh), 1237.7 (w, sh), 1205.0 (w, sh), 1161.0 (w, sh), 1103.6 (st, sh), 1070.9 (s, br), 1008.9 (m, sh), 928.1 (w, sh), 790.5 (m, br), 743.2 (w), 690.7 (m, sh), 669.5 (m, sh), 624.4 (m, sh), 574.0 (m), 547.7 (m), 530.8 (m), 478.9 (m), 453.1 (m), 443.9 (m), 434.5 (m) [where: st (strong), m (medium), w (weak); and: broad (br), sharp (sh)].

Route 1: The indirect attachment of the Mn_4 cluster to the nanotubes was accomplished through a two-step process: 1) introduction of carboxylic groups to the MWNTs and their further deprotonation in basic medium, and 2) combination of the cationic Mn_4 complex with the previously generated anionic nanotubes.

Functionalization of MWNTs with Carboxylic Groups: Typically, MWNTs (3 g) in HNO_3 (420 mL; 2.6 M) was heated under reflux for 4.5 h. The mixture was then cooled to room temperature and centrifuged before the supernatant acid was decanted off. The resulting black solid was resuspended in water and centrifuged, and this process repeated until the pH of the supernatant reached neutrality. Finally, deprotonation of the as-prepared MWNT-COOH was accomplished by resuspending it in water (500 mL) containing Titron X-100 surfactant (7 mL), and carefully adding sodium hydroxide (aqueous solution, 1 M) until pH 10 was achieved. Finally the carbon-based material was filtered off under vacuum over a cellulose nitrate membrane (pore size 0.8 µm) and thoroughly cleaned with deionized water.

The concentration of carboxylic groups was estimated through acid–base titration.[13,22] In a typical procedure, MWNT-COOH (50 mg) was suspended in $NaHCO_3$ (aq; 25 mL) and stirred for 48 h. The deprotonated nanotubes were filtered off over a cellulose nitrate membrane, and washed with deionized water. Finally, HCl (aq; 25 mL; 0.05 M) was added to the filtered solution and the mixture was boiled for 20 min to degas it. The excess acid was back titrated by using NaOH (aq; 0.05 M).

*Preparation of the Mn_4-MWNT Hybrid (**1**)*: The previously deprotonated MWNT-COO^- (4 mg) was suspended in acetonitrile (40 mL), and subjected to sequential ultrasound cycles for 30 min.

Next, $[Mn_4(OAc)_2(pdmH)_6](ClO_4)_2$ (10 mg; 7 µmol) was added, and the brownish mixture mechanically stirred at room temperature for 3 days. Finally, the carbon-based black solid was filtered in vacuo over a PTFE membrane, washed thoroughly with acetonitrile and dried under vacuum.

Additional experiments were undertaken to clarify the critical importance that the cleaning protocol used has in determining the nature of the resulting hybrid nanocomposite. In this regard, a small fraction of the hybrid **1** was separated after the Mn_4 loading and subjected to softer cleaning, which did not include continuous ultrasound cycles. SI 4 in the Supporting Information displays a more bundled material accompanied by the presence of numerous dark islands, which, on basis of the EDS analysis, turned out to be mainly composed of manganese, which indicates that the main part of the Mn_4 cluster added was coprecipitated but not directly attached to the carbon material. This heterogeneous distribution is far from ideal; the molecular component must be exclusively grafted on the MWNTs, and hence substantial effort was devoted to the removal of these contaminant islands via exhaustive cleaning protocols.

Route 2: Direct attachment of the Mn_4 cluster to the nanotubes was accomplished in one step by combining the cationic complex with anionic MWNTs generated in situ.

*Preparation of the Mn_4-MWNT Hybrid (**2**)*. According to a previously reported method,[23] granular lithium (7 mg; 1 mmol) was added to an argon-purged flask containing MWNT (12 mg; commercial grade) and DTBP (26 mg; 0.1 mmol) in THF (10 mL; anhydrous). The mixture was sonicated for 1 h to facilitate lithium dissolution. Once the metal was dissolved, a solution of the Mn_4 cluster (100 mg; 70 µmol) in acetonitrile (5 mL) was added and the mixture subjected to continuous sonication at room temperature overnight. After evaporation of the solvent under reduced pressure, the black solid was thoroughly washed successively with dichloromethane and acetonitrile, and finally filtrated in vacuo over a PTFE membrane.

Physical Characterization: FTIR spectra were acquired on a FTIR Nicolet 5700 spectrometer in the 4000–400 cm^{-1} frequency range using powdered samples diluted in KBr pellets.

TGA was carried out with a Mettler Toledo TGA/SDTA 851 apparatus in the 25–800 °C temperature range under a 30 mL mol^{-1} air flow at a 10 K min^{-1} scan rate.

Electron spectroscopy for chemical analysis (ESCA) and XPS were performed using a Thermo Scientific K-Alpha ESCA instrument equipped with aluminium Kα1,2 monochromatized radiation at 1486.6 eV X-ray source. The nonconductive nature of the samples required the use of an electron flood gun to minimize surface charging. Neutralization of the surface charge was performed by using a low energy flood gun (electrons in the range 0 to 14 eV) and a low Argon ions gun. The XPS measurements were carried out using monochromatic Al-K radiation ($h\nu$ = 1486.6 eV). Photoelectrons were collected from a take-off angle of 90° relative to the sample surface. The measurement was done in a constant analyser energy mode (CAE) with a 100 eV pass energy for survey spectra and 20 eV pass energy for high resolution spectra. Charge referencing was done by setting the lower binding energy C 1s photo peak at 285.0 eV C1s hydrocarbon peak.[24] Surface elemental composition was determined using the standard Scofield photoemission cross sections.

HRTEM images were obtained with a JEOL JEM 2010F HRTEM. HAADF-STEM images show mass–thickness contrast, where the brighter areas correspond to the presence of heavier elements; these images were obtained by coupling the annular detector to the STEM unit. STEM-EDS elemental maps show the relative distribution of the elements, and were obtained by coupling the STEM unit to the EDS detector. In the images, the red areas correspond to C (C Kα line), and the green areas correspond to Mn (Mn Kα line); the background was subtracted in the map.

AFM images were taken using an AFM commercial multimode III from Veeco. The MWNTs were deposited into a HOPG surface, and the measurements were taken using a silica tip (frequency 300KHz, K = 40 N m^{-1}) at room temperature in ambient conditions.

Magnetic measurements were performed using a Quantum Design SQUID Magnetometer MPMS-XL-5. The direct current (DC) data were collected under an external applied field of 1000 G in the 2–300 K temperature range. The susceptibility data were corrected from the diamagnetic contributions of the atomic constituents of the samples, as deduced by using Pascal's constant tables and the sample holder. Magnetization studies were performed between -5 and +5 T at a constant temperature of 2 K. The dynamic AC susceptibility data were collected in the 2–14 K range with an applied alternating field of 3.95 G at various frequencies between 1 and 333 Hz.

Supporting Information

Supporting Information is available from the Wiley Online Library or from the author.

Acknowledgements

Financial support from the EU (Projects ELFOS and ERC Advanced Grant SPINMOL), the Spanish Ministerio de Ciencia e Innovación (Project Consolider-Ingenio in Molecular Nanoscience and projects MAT2007-61584 and CTQ-2008-06720, co-financed by FEDER), and the Generalitat Valenciana (Prometeo Program) are gratefully acknowledged. CMG thanks the EU for a Marie Curie Fellowship (IEF-253369). The authors also acknowledge E. Pinilla-Cienfuegos and J. M. Martínez for AFM studies and magnetic measurements, respectively.

Received: September 19, 2011
Published online: January 9, 2012

[1] a) R. Sessoli, D. Gatteschi, A. Caneschi, M. A. Novak, *Nature* **1993**, *365*, 141; b) D. Gatteschi, R. Sessoli. *Angew. Chem. Int. Ed.* **2003**, *42*, 268.
[2] a) N. Ishikawa, M. Sugita, T. Ishikawa, S. Koshihara, Y. J. Kaizu, *J. Am. Chem. Soc.* **2003**, *125*, 8694; b) M. A. Aldamen, J. M. Clemente-León, E. Coronado, C. Martí-Gastaldo, A. Gaita-Ariño, *J. Am. Chem. Soc.* **2008**, *130*, 8874.
[3] a) E. Coronado, J. Camarero, *J. Mater. Chem.* **2009**, *19*, 1678; b) M. N. Leuenberger, D. Loss, *Nature* **2001**, *410*, 789.
[4] L. Bogani, W. Wernsdorfer, *Nat. Mater.* **2008**, *7*, 179.
[5] a) P. G. Collins, K. Bradley, M. Ishigami, A. Zettl, *Science* **2000**, *287*, 1801; b) S. Sanvito, A. R. Rocha, *J. Comput. Theor. NanoSci.* **2006**, *3*, 624; c) B. L. Allen, P. D. Kichambare, A. Star, *Adv. Mater.* **2007**, *19*, 1439.
[6] A. Giusti, G. Charron, S. Mazerat, J.-D. Compain, P. Mialane, A. Dolbecq, E. Rivière, W. Wernsdorfer, R. N. Biboum, B. Keita, L. Nadjo, A. Filoramo, J.-P. Bourgoin, T. Mallah, *Angew. Chem. Int. Ed.* **2009**, *48*, 4949.
[7] a) L. Bogani, C. Danieli, E. Biavardi, N. Bendiab, A.-L. Barra, E. Dalcanale, W. Wernsdorfer, A. Cornia, *Angew. Chem. Int. Ed.* **2009**, *48*, 746; b) S. Kyatskaya, J. R. Galán-Mascarós, L. Bogani, F. Henrich, M. Kappes, W. Wernsdorfer, M. Ruben, *J. Am. Chem. Soc.* **2009**, *131*, 15143.
[8] J. Yoo, E. K. Brechin, A. Yamaguchi, M. Nakano, J. C. Huffman, A. L. Maniero, L.-C. Brunel, K. Awaga, H. Ishimoto, G. Christou, D. N. Hendrickson, *Inorg. Chem.* **2000**, *39*, 3615.
[9] H. Miyasaka, K. Nakata, K. Sugiura, M. Yamashita, R. Clerac, *Angew. Chem. Int. Ed.* **2004**, *43*, 707.
[10] a) B. K. Price, J. R. Lomeda, J. M. Tour, *Chem. Mater.* **2009**, *21*, 3917; b) B. Smith, K. Wepasnick, K. E. Schrote, H-H. Cho, W. P. Ball, D. H. Fairbrother, *Langmuir* **2009**, *25*, 9767.
[11] H. Peng, L. B. Alemany, J. L. Margrave, V. N. Khabashesku, *J. Am. Chem. Soc.* **2003**, *125*, 15174.

[12] H. Igarashi, H. Murakami, Y. Murakami, S. Maruyama, N. Nakashima, *Chem. Phys. Lett.* **2004**, *392*, 529.
[13] H. Hu, P. Bhowmik, B. Zhao, M. A. Hamon, M. E. Itkis, R. C. Haddon, *Chem. Phys. Lett.* **2001**, *345*, 25.
[14] L. Bogani, W. Wernsdorfer, *Inorg. Chim. Acta* **2008**, *361*, 3807.
[15] M. Fukiwara, T. Matsushita, S. Ikeda, *J., Electron Spectrosc. Relat. Phenom.* **1995**, *74*, 201.
[16] V. Dicastro, G. Polzonetti, *J. Electron Spectrosc. Relat. Phenom.* **1989**, *48*, 117.
[17] G. Charron, A. Giuti, S. Mazerat, P. Mialane, A. Gloter, F. Miserque, B. Keita, L. Nadjo, A. Filoramo, E. Rivière, W. Wernsdorfer, V. Huc, J.-P. Bourgoin, T. Mallah, *Nanoscale* **2010**, *2*, 139.
[18] I. S. Jacobs, *J. Phys. Chem. Solids* **1959**, *11*, 1.
[19] G. Srinivisan, M. S. Seehra, *Phys. Rev. B* **1983**, *28*, 6542.
[20] M. Regulski, R. Przenioslo, I. Sosnowska, D. Holwein, R. Schneider, *J. Alloy Compd.* **2004**, *362*, 236.
[21] J. B. Vincent, H.-R. Chang, K. Folting, J. C. Huffman, G. Christou, D. N. Hendrickson, *J. Am. Chem. Soc.* **1987**, *109*, 5703.
[22] S. C. Tsang, Y. K. Chen, P. J. F. Harris, M. L. H. Green, *Nature* **1994**, *372*, 159.
[23] A. García-Gallastegui, I. Obieta, I. Bustero, G. Imbuluzqueta, J. Arbiol, J. I. Miranda, J. M. Aizpurua, *Chem. Mater.* **2008**, *20*, 4433.
[24] D. Briggs, M. P. Seah, *Practical Surface Analysis Vol.* 1, 2 ed., Wiley, 1990.